CrossMark

Synergistic Effects of Ag Nanoparticles/BiV$_{1-x}$Mo$_x$O$_4$ with Enhanced Photocatalytic Activity

Mengting Yu[1], Shixiong Zhou[1], Qingguo Meng[2], Haiqin Lv[2], Zhihong Chen[2,3*], Yongguang Zhang[3], Mingliang Jin[1,3], Mingzhe Yuan[2], Xin Wang[1,3*] (ID) and Guofu Zhou[1,3]

Abstract

In recent years, BiVO$_4$ has drawn much attention as a novel photocatalyst given its excellent ability to absorb visible light. This work reports the development of Ag-modified BiV$_{1-x}$Mo$_x$O$_4$ composites through a facile hydrothermal synthesis with the subsequent photoinduced reduction of Ag$^+$ at almost neutral pH conditions. Metallic Ag nanoparticles were deposited on the (040) facet of Mo-doped BiVO$_4$ powders. The crystal structure and morphology of the as-prepared samples were studied by XRD and SEM analyses. Moreover, the photocatalytic performance of BiVO$_4$, Ag/BiVO$_4$, and Ag-modified BiV$_{1-x}$Mo$_x$O$_4$ were evaluated by the degradation of rhodamine B (RhB). The Ag/BiV$_{0.9925}$Mo$_{0.0075}$O$_4$ composite exhibited the most efficient photocatalytic performance. The present work provides greater insight into the application of BiVO$_4$ in the field of photocatalysis.

Keywords: Hydrothermal synthesis, Photocatalytic, Metal doping, Ag/BiV$_{1-x}$Mo$_x$O$_4$

Background

Given the increasing environmental pollution and energy crises, the development of efficient and promising solutions to reduce energy shortages and protect the environment is paramount [1, 2]. Photocatalyst-based semiconductors, such as Bi$_2$WO$_6$ [3, 4], BiPO$_4$ [5, 6], Ag$_3$PO$_4$ [7, 8], and BiVO$_4$ [9–13], have attracted much attention due to their applications in the degradation of organic pollutants or hydrogen production from water splitting. Nevertheless, most of the existing oxide photocatalysts have very low light-response efficiencies primarily because they only respond to ultraviolet light due to their narrow bandgaps [14–16]. Additionally, the photoinduced electrons can easily recombine with holes leading to a lower optical performance [17, 18].

Due to its visible photocatalytic activity, wide bandgap of 2.42 eV, high stability, and non-toxicity, bismuth vanadate (BiVO$_4$) is a promising n-type semiconductor photocatalyst [19–21]. However, its resulting carrier transfer efficiency is relatively poor, leading to the recombination of photogenerated electrons and holes, which severely limits the photocatalytic performance of BiVO$_4$. Various studies have assessed BiVO$_4$ modifications [20, 22–24], and substitution or metal doping on BiVO$_4$ has been shown as the most efficient method to change its carrier transport efficiency. Metal element doping introduces new defects or charges in the crystal lattice [25], influencing the motion of electrons and the creation of holes under light irradiation [26, 27]. Adjustments to the distribution status or changes in the band structures can lead to changes in the activity of semiconductors [28]. For example, Thalluri et al. [29] introduced hexavalent molybdenum (Mo) at an almost neutral pH to substitute V while preserving the atomic ratio of fBiVO$_4$, leading to the formation of a good crystal structure and considerable photocatalytic activity for water oxidation. Mo has a higher valence than V and therefore strengthens the n-type characteristics of the material [30]. Additionally, the photocatalytic activity of BiVO$_4$ is highly dependent on its various crystal facets. Recent studies on the deposition of noble metals, such as Ag, Cu, and Au, on the different facets of BiVO$_4$ have

* Correspondence: chenzhihong1227@sina.com; wangxin@scnu.edu.cn
[2]Shenyang Institute of Automation, Chinese Academy of Sciences, Guangzhou 511458, China
[1]South China Academy of Advanced Optoelectronics, South China Normal University, Guangzhou, Guangdong Province, China
Full list of author information is available at the end of the article

Yu *et al. Nanoscale Research Letters* (2017) 12:588

Page 2 of 10

demonstrated good photocatalytic activity [31–33]. Li et al. [34] produced an Ag/BiVO$_4$ composite through the hydrothermal synthesis and photoreduction of Ag deposited on the (040) crystal facets of BiVO$_4$, leading to an enhanced photoelectrochemical performance, as indicated by the fast separation of the electron–hole pairs.

In the present study, we build on the facile hydrothermal synthesis approach of Li et al. [29] to obtain BiV$_{0.9925}$Mo$_{0.0075}$O$_4$ in weakly alkaline conditions, coupled with photoreduction deposition of Ag nanoparticles on the (040) facets of the as-produced substrate materials. Ag/BiV$_{0.9925}$Mo$_{0.0075}$O$_4$ composite photocatalysts were successfully synthesized and showed enhanced photocatalytic degradation of rhodamine B (RhB) under xenon lamp irradiation ($\lambda > 420$ nm) compared to the non-composite Ag-deposited or Mo-doped BiVO$_4$ materials. Herein, we report the preparation, characterization, and photocatalytic activity of BiVO$_4$, Ag/BiVO$_4$, BiV$_{1-x}$Mo$_x$O$_4$, and Ag/BiV$_{1-x}$Mo$_x$O$_4$ composites.

Experimental

Synthesis of BiVO$_4$ and BiV$_{1-x}$Mo$_x$O$_4$ Powders

Bismuth nitrate pentahydrate (Bi(NO$_3$)$_3$·5H$_2$O, analytical grade), ammonium metavanadate (NH$_4$VO$_3$, analytical grade), ammonium carbonate, and ammonium molybdate ((NH$_4$)$_2$MoO$_4$) were obtained from Sigma–Aldrich and used as received, without any further purification. All other chemicals used in the experiments were also of analytical grade, and deionized water was used for the preparation of the solutions. In a typical process, 3.7 mmol of Bi(NO$_3$)$_3$·5H$_2$O, 3.7 mmol of NH$_4$VO$_3$, and 12 mmol of (NH$_4$)$_2$CO$_3$ were dissolved in 75 mL of 1 M HNO$_3$ and stirred for approximately 30 min at room temperature until a clear solution was obtained. The pH of the mixture was adjusted to pH 8 with NaOH (2 M). The mixture was transferred into a 150-mL Teflon-lined stainless autoclave and heated for 12 h at 180 °C under autogenous pressure in an oven. The precipitate was filtered and washed three times with distilled water followed by ethanol and dried for 12 h at 60 °C in a drying oven.

The doped samples were prepared by replacing the equivalent weight of NH$_4$VO$_3$ with different amounts of Mo. Mo precursors were introduced such that a nominal 0.5, 0.75, and 1% atomic substitution of V was achieved.

Preparation of Ag/BiVO$_4$ and Ag/BiV$_{1-x}$Mo$_x$O$_4$ Samples

BiVO$_4$ (0.50 g) and AgNO$_3$ (0.05 g) were added to a (NH$_4$)$_2$C$_2$O$_4$ (0.8 g L^{-1}, 100 mL) aqueous solution in a 250-mL beaker in an ultrasonic bath until an evenly dispersed solution was formed. The resulting yellow mixture was then irradiated with a Xenon lamp for 30 min under magnetic stirring. The color of the system

turned from a vivid yellow to grayish-green, indicating the generation of metallic Ag in the reaction system. The resulting samples were then filtered, washed with DI water, and dried at 60 °C for 12 h to obtain the Ag/BiVO$_4$ and Ag/BiV$_{1-x}$Mo$_x$O$_4$ composites.

Photocatalytic Activity

Assessment of the photocatalytic activity was performed using the degradation rate of RhB. The experimental system for photodegradation was calibrated at a UV cut-off wavelength below 420 nm, and the irradiation height of the Xenon lamp was close to the height of the 250-mL beaker. In a typical procedure, the as-prepared photocatalyst (0.1 g) was well dispersed in a RhB aqueous solution (150 mL, 10 mg L^{-1}) under ultrasonication in a glass reactor equipped with a cooling water circulator to maintain a reaction system temperature of room temperature. The suspension was stirred for 30 min in the dark to reach the adsorption–desorption equilibrium and was then irradiated for 2 h with a Xenon lamp (300 W) under continuous stirring. A 5-mL aliquot of the suspension was taken every 30 min and centrifuged. The absorption spectrum of the obtained liquid
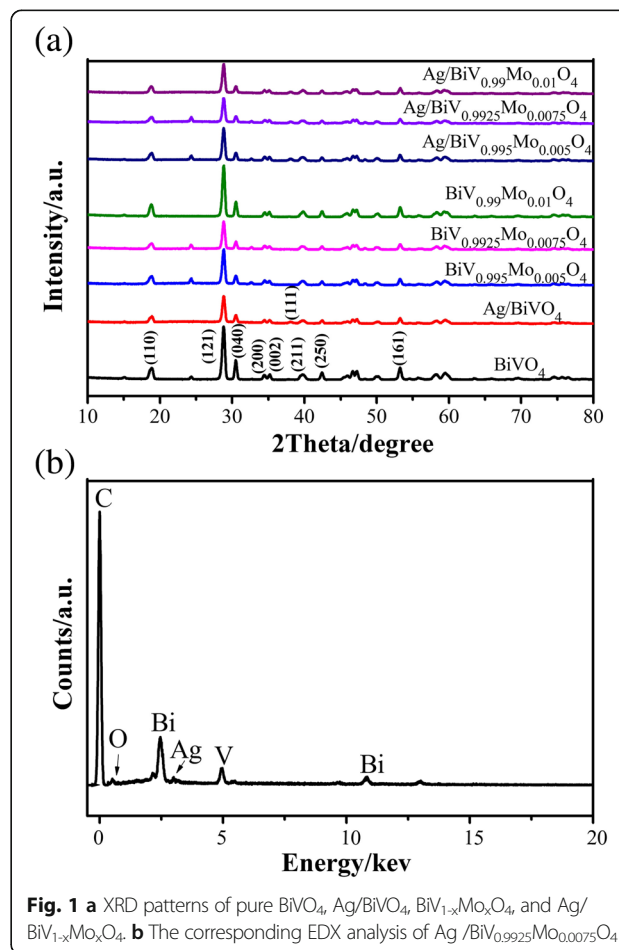

Fig. 1 a XRD patterns of pure BiVO$_4$, Ag/BiVO$_4$, BiV$_{1-x}$Mo$_x$O$_4$, and Ag/BiV$_{1-x}$Mo$_x$O$_4$. **b** The corresponding EDX analysis of Ag /BiV$_{0.9925}$Mo$_{0.0075}$O$_4$
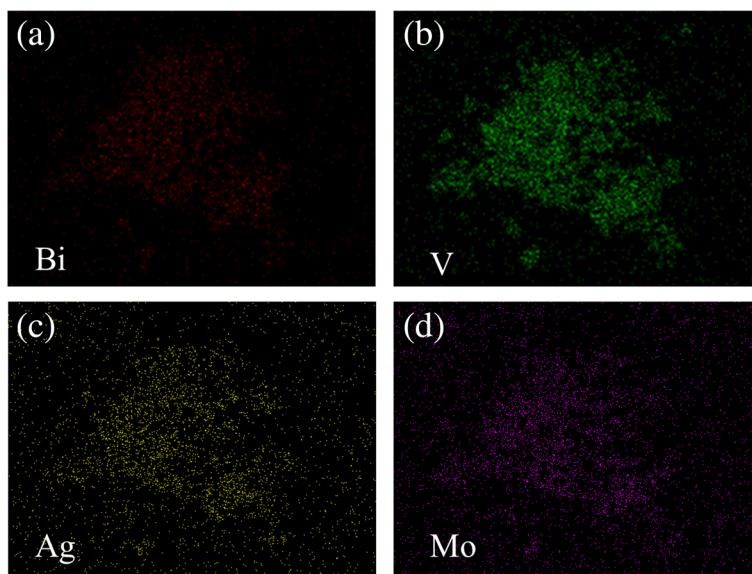
Yu et al. Nanoscale Research Letters (2017) 12:588

Page 3 of 10

Fig. 2 a–d The corresponding elemental mapping analysis of Bi, V, Ag, and Mo in $Ag/BiV_{0.9925}Mo_{0.0075}O_4$, respectively

supernatant was measured in reference to the absorption intensity of RhB at 552 nm.

Characterization Techniques

The morphologies of the pure $BiVO_4$ and the decorated composites were investigated by field emission scanning electron microscopy (FESEM, S4800) and transmission electron microscopy (TEM; JEM-2100F, JEOL). Elemental analysis was performed by X-ray photoelectron spectroscopy (XPS; VGESCA-LAB MKII) with a non-monochromatic Mg Kα X-ray source. The crystalline phase of the samples was determined by X-ray diffraction (XRD; Bruker D8) with Cu Kα radiation. Inductively coupled plasma (ICP) was employed to analyze the elemental composition of the samples. Additionally, UV–vis diffuse reflectance spectrum measurements were performed using a Shimadzu spectrophotometer (UV-2450) to evaluate the bandgap energy of $BiVO_4$, $Ag/BiVO_4$, $BiV_{1-x}Mo_xO_4$, and $Ag/BiV_{1-x}Mo_xO_4$ over a wavelength range of 360–800 nm.

Results and Discussion

The crystallographic structure and phase of the prepared composites were characterized by XRD analysis (Fig. 1a).

The sharp diffraction peaks observed in the as-prepared BiVO4 were assigned to the conventional $BiVO_4$ phase since they were in good agreement with the standard (JCPDS) card no. 14-0688. According to the peak splitting observed at 18.7° and 30.5°, which indicate the (110) and (040) facets, the prepared $BiVO_4$ material possessed a single monoclinic scheelite structure. A diffraction peak at 38.1° was observed in the Ag-related photocatalysts (Fig. 1a) corresponding to the (111) crystal phase of metallic Ag (JCPDS file: 65-2871). This indicates that the photoreduction of Ag^+ ions indeed occurred, leading to the deposition of Ag nanoparticles on the $BiVO_4$ and $BiV_{1-x}Mo_xO_4$ surfaces. Nevertheless, due to the low relative content of Ag, the XRD peaks were not intense.

As shown in Fig. 2a, EDS confirmed the presence of the Ag species, which agrees with the XRD results. The Bi (Fig. 2b), O (Fig. 2c), V (Fig. 2d), Mo (Fig. 2e), and Ag (Fig. 2f) elements are all distributed uniformly in the $Ag/BiV_{1-x}Mo_xO_4$ composites, and the results verify the existence of Mo and Ag. The relative amounts of Mo did not appear to affect the crystal structure or phase. The Mo substitution ratio was assessed by ICP (Table 1); the practical Mo atomic content was calculated to be 0.16% in $Ag/BiV_{0.9925}Mo_{0.0075}O_4$. It was observed that,

Table 1 Properties of the pure $BiVO_4$, $Ag/BiVO_4$, $BiV_{0.9925}Mo_{0.0075}O_4$, and $Ag/BiV_{0.9925}Mo_{0.0075}O_4$ powders

Sample	$BiVO_4$	$Ag/BiVO_4$	$BiV_{0.9925}Mo_{0.0075}O_4$	$Ag/BiV_{0.9925}Mo_{0.0075}O_4$
Bandgap (eV)	2.30	1.61	2.18	1.78
Atomic% of Ag dopant from ICP	–	6.28446	–	5.92476
Atomic% of Mo dopant from ICP	–	–	0.163704	0.167735
Atomic% of Ag dopant from XPS	–	6.03	–	4.72
Degradation rate (%)	6.4	8.4	9.6	97.9

Yu et al. Nanoscale Research Letters (2017) 12:588
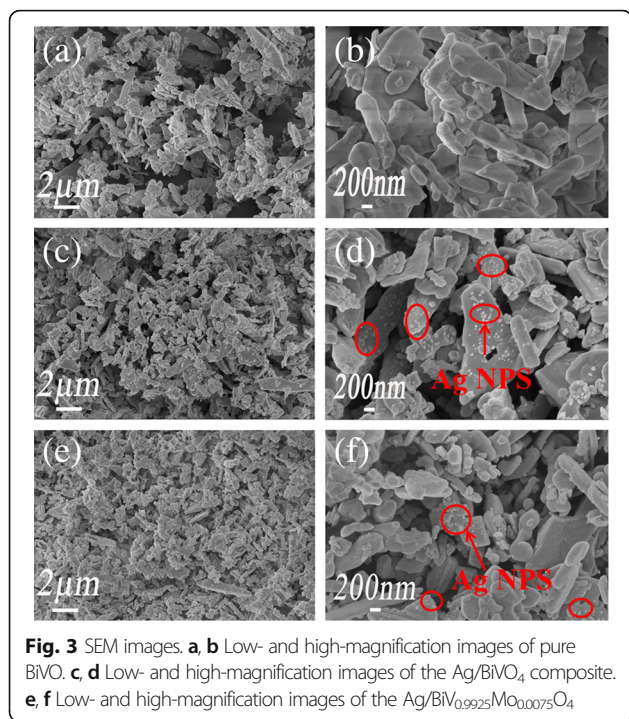
Page 4 of 10

Fig. 3 SEM images. **a**, **b** Low- and high-magnification images of pure BiVO. **c**, **d** Low- and high-magnification images of the Ag/BiVO$_4$ composite. **e**, **f** Low- and high-magnification images of the Ag/BiV$_{0.9925}$Mo$_{0.0075}$O$_4$

although the nominal dopant content introduced with the precursors was 0.75%, the final resulting amount of Mo in the doped materials was always lower than the expected. Similar results have also been found in previous research, and it is possible that intrinsic losses and the evaporation of the Mo dopant occur during the hydrothermal synthesis processes [35, 36].

The morphology of the as-prepared pure BiVO$_4$, Ag/BiVO$_4$, and Ag/BiV$_{1-x}$Mo$_x$O$_4$ were investigated by SEM (Fig. 3). Pure BiVO$_4$ showed a slice-layer morphology with several clusters (Fig. 3a, b). For Ag/BiVO$_4$, metallic Ag was observed to be well dispersed on the (040) crystal facet (Fig. 3c), which agrees with the XRD analysis. The images of Ag/BiV$_{0.9925}$Mo$_{0.0075}$O$_4$ composite at different magnification were shown in Fig. 3e, d. Uniformly shaped metallic Ag nanoparticles were clearly observed on the surface of Ag/BiV$_{0.9925}$Mo$_{0.0075}$O$_4$ (Fig. 3d) likely due to the high exposure of the (040) surface. This crystal facet has been shown to have a good charge carrier mobility [37]. Thus, the observed morphology should be beneficial to the photocatalytic performance of the synthesized doped BiVO$_4$ powders. The as-prepared BiVO$_4$, Ag/BiVO$_4$, and Ag/BiV$_{0.9925}$Mo$_{0.0075}$O$_4$ samples were further observed by TEM (Fig. 4a). Interplanar spacings of 0.475 nm were clearly observed in Fig. 4b, corresponding to the (110)
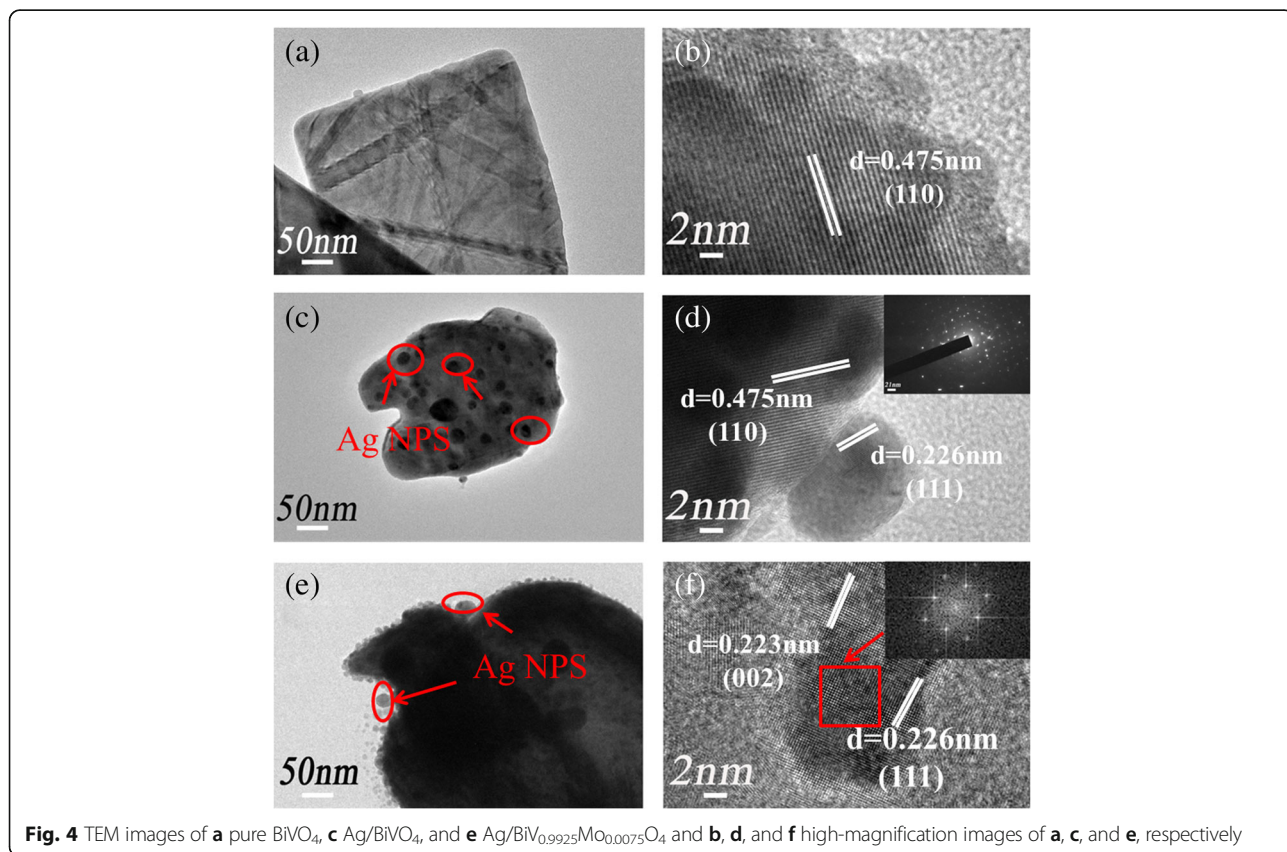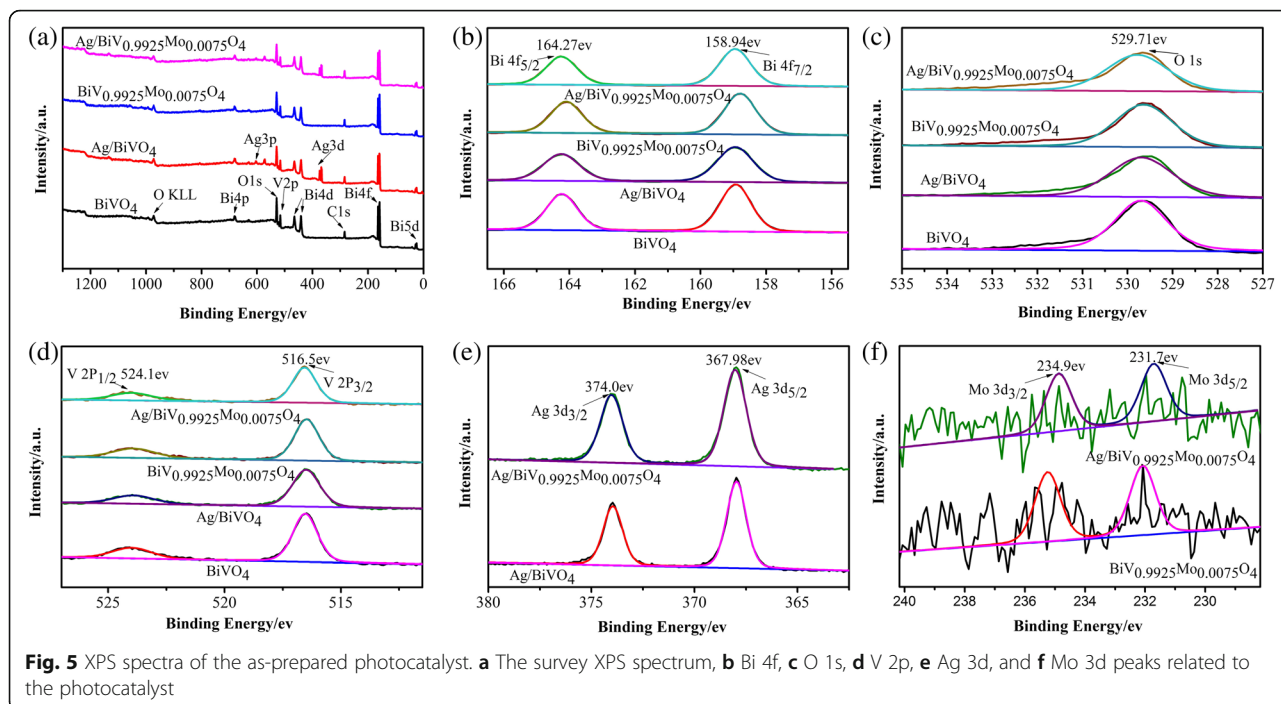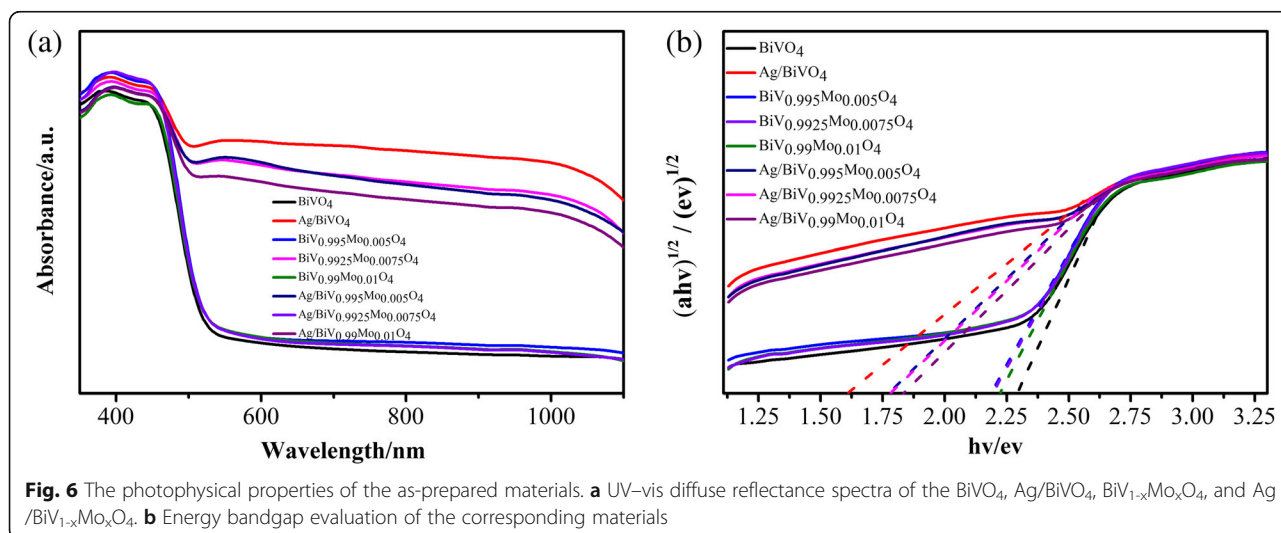

Fig. 4 TEM images of **a** pure BiVO$_4$, **c** Ag/BiVO$_4$, and **e** Ag/BiV$_{0.9925}$Mo$_{0.0075}$O$_4$ and **b**, **d**, and **f** high-magnification images of **a**, **c**, and **e**, respectively

Yu *et al. Nanoscale Research Letters* (2017) 12:588

Page 5 of 10

Fig. 5 XPS spectra of the as-prepared photocatalyst. **a** The survey XPS spectrum, **b** Bi 4f, **c** O 1s, **d** V 2p, **e** Ag 3d, and **f** Mo 3d peaks related to the photocatalyst

crystallographic facet of $BiVO_4$ (JCPDS Card No. 14-0688). The crystal lattice fringe at 0.226 nm belonged to the (111) plane of metallic Ag nanoparticles in the $Ag/BiVO_4$ and $Ag/BiV_{0.9925}Mo_{0.0075}O_4$ samples (Fig. 4d, f). Based on the above analyses, metallic Ag was successfully deposited onto the $BiV_{0.9925}Mo_{0.0075}O_4$ surface, leading to a good connection between Ag and the Mo-doped $BiVO_4$ and promoting effective electron and hole separation in the composite system.

XPS analysis of the as-prepared samples confirmed the presence of Bi, V, O, Ag, and Mo (Fig. 5a). The binding energies of Bi 4f were 158.94 and 164.27 eV,

corresponding to Bi $4f^{7/2}$ and $4f^{5/2}$, respectively, confirming the Bi^{3+} peaks in $BiVO_4$ (Fig. 5b). A typical O 1s spectrum was observed, as indicated by the main characteristic peak at 529.71 eV (Fig. 5c). The V $2p^{3/2}$ and $2p^{1/2}$ peaks observed at 516.5 and 524.1 eV, respectively, indicated the existence of V^{5+} (Fig. 5d). The Ag 3d peaks at 367.98 and 374.0 eV, corresponding to Ag $3d^{5/2}$ and $3d^{3/2}$ (Fig. 5e), respectively, were observed in both $Ag/BiVO_4$ and $Ag/BiV_{0.9925}Mo_{0.0075}O_4$, confirming the existence of the metallic Ag species. Furthermore, the molar ratio of metallic Ag species accounted for 6.6% of all elements, as determined by XPS and in agreement with

Fig. 6 The photophysical properties of the as-prepared materials. **a** UV–vis diffuse reflectance spectra of the $BiVO_4$, $Ag/BiVO_4$, $BiV_{1-x}Mo_xO_4$, and $Ag/BiV_{1-x}Mo_xO_4$. **b** Energy bandgap evaluation of the corresponding materials

Yu *et al. Nanoscale Research Letters* (2017) 12:588

Page 6 of 10

the ICP measurements (Table 1). Finally, the Mo $3d^{5/2}$ and $3d^{3/2}$ peaks located at 231.7 and 234.9 eV (Fig. 5f), respectively, confirm the presence of Mo^{6+}.

UV–vis diffuse reflectance spectrum measurements were taken to evaluate the optical bandgap and absorption properties of the photocatalysts, as shown in Fig. 5. The photocatalytic activity of a semiconductor is largely dependent on the size of the bandgap; the narrower the bandgap is, the greater the shift is of the absorption wavelength towards longer wavelengths. The bandgap of as-prepared $BiVO_4$ was approximately 2.3 eV (Fig. 6b), which agrees with the Kubelka–Munk bandgap estimation theory [38]. Compared with $BiVO_4$, all the Mo-doped samples showed relatively narrow bandgaps (Fig. 6b). Furthermore, all Ag-deposited $BiVO_4$ and $BiV_{1-x}Mo_xO_4$ photocatalysts exhibited strong absorption in the visible light range in Fig. 6a. The $Ag/BiVO_4$ photocatalyst exhibited the best light absorption. The absorbance of as-prepared $Ag/BiV_{0.9925}Mo_{0.0075}O_4$ was between that of $BiVO_4$ and $Ag/BiVO_4$, thus indicating that the introduction of Mo hindered the photoresponsive characteristics of Ag. However, it is worth pointing out that, in addition to photoabsorption, other characteristics can also significantly influence the photocatalytic efficiency of photocatalysts.

Photoluminescence (PL) spectras were taken to investigate the separation efficiency of the photogenerated electron–hole pairs. The PL spectra of pure $BiVO_4$, $BiV_{0.9925}Mo_{0.0075}O_4$, $Ag/BiVO_4$, and $Ag/BiV_{0.9925}Mo_{0.0075}O_4$ composites, with an excitation wavelength of 310 nm, are shown in Fig. 7. $BiVO_4$ and $BiV_{0.9925}Mo_{0.0075}O_4$ show a prominent emission band centered at approximately 510 nm. The order of the intensity of the PL spectra was $BiVO_4 > BiV_{0.9925}Mo_{0.0075}O_4 > Ag/BiVO_4 > Ag/BiV_{0.9925}Mo_{0.0075}O_4$. Because a lower PL intensity
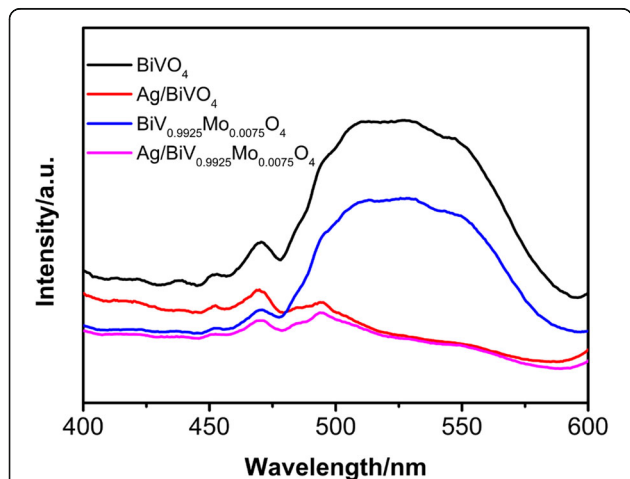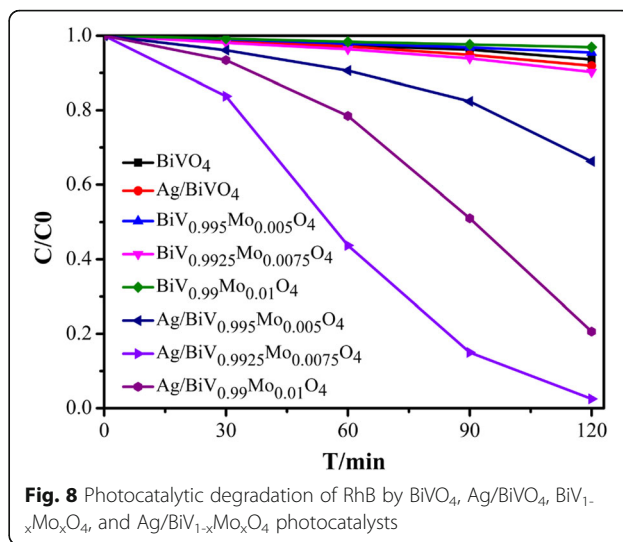
Fig. 8 Photocatalytic degradation of RhB by $BiVO_4$, $Ag/BiVO_4$, $BiV_{1-x}Mo_xO_4$, and $Ag/BiV_{1-x}Mo_xO_4$ photocatalysts

indicates a higher separation efficiency, this would lead to a higher photocatalytic activity in the overall system. Consequently, the higher photocatalytic performance of $Ag/BiV_{0.9925}Mo_{0.0075}O_4$ agrees with the PL measurement.

The photocatalytic decomposition results, according to the degradation of RhB under visible light ($\lambda > 420$ nm), confirmed Ag or Mo alone had little effect on the catalytic activity of $BiVO_4$ under light irradiation for 2 h (Fig. 8). Conversely, the deposition of Ag on Mo-doped $BiVO_4$ showed effective photocatalytic activity, with the variation of the Mo content, showing a difference in photocatalytic activity. $Ag/BiV_{0.9925}Mo_{0.0075}O_4$ exhibited an extremely efficient degradation of RhB under visible light irradiation with full decolorization after 2 h while only 7, 8, and 10% degradation was achieved over $BiVO_4$, $Ag/BiVO_4$, and $BiV_{0.9925}Mo_{0.0075}O_4$, respectively. Thus, Mo-doped Ag-deposited $BiVO_4$ was able to suppress the charge
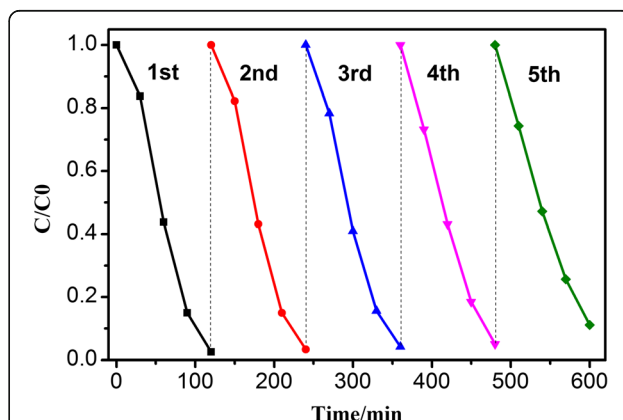
Fig. 7 Photoluminescence spectra of pristine $BiVO_4$, $Ag/BiVO_4$, $BiV_{0.9925}Mo_{0.0075}O_4$, and $Ag/BiV_{0.9925}Mo_{0.0075}O_4$ composites

Fig. 9 Five cycle runs of $Ag/BiV_{0.9925}Mo_{0.005}O_4$ for the photodegradation of RhB under visible light irradiation

Yu *et al. Nanoscale Research Letters* (2017) 12:588

Page 7 of 10

recombination and greatly enhance the efficiency of the photocatalytic process.

The stability and reusability of photocatalysts are very important for their practical application. Therefore, we assessed the repeated cycles of $Ag/BiV_{0.9925}Mo_{0.0075}O_4$ in the photocatalytic degradation of RhB for 2 h under visible light irradiation. Overall, 99% of the RhB solution was degraded after five cycles (Fig. 9), indicating that the sample exhibited good photocatalytic stability.

To further assess the separation efficiency, the charge carrier lifetimes of pure $BiVO_4$, $Ag/BiVO_4$, and $Ag/BiV_{0.9925}Mo_{0.0075}O_4$ were also analyzed (Fig. 10). The

decay curves for the as-prepared photocatalysts fit well to a double-exponential function. The charge carrier decay lifetimes of $BiVO_4$, $Ag/BiVO_4$, and $Ag/BiV_{0.9925}Mo_{0.0075}O_4$ composites were 1.2304, 1.8220, and 2.0933 ns, respectively. Thus, the Ag-deposited samples, both with and without Mo doping, had much longer charge carrier lifetimes than pure $BiVO_4$, achieving effective photocarrier separation and suggesting that a synergistic effect among Ag, Mo, and $BiVO_4$ led to enhancements of the photocatalytic activity.

To explore the underlying photocatalytic mechanism, RhB degradation was conducted under visible light irradiation [39], adding a hole (h^+) scavenger (ammonium oxalate ($(NH_4)_2C_2O_4$)), a superoxide radical ($\cdot O^{2-}$) scavenger (1.4-benzoquinone, BQ) [40], or hydroxyl radical ($\cdot OH$) scavengers (tert-Butanol, t-BuOH) [41]. Following the addition of BQ, no obvious decrease was observed, but an acceleration in the degradation rate was detected compared to that of $Ag/BiV_{0.9925}Mo_{0.0075}O_4$ (Fig. 11). The faster degradation rate may have resulted from the SPR-effect of metallic Ag in $Ag/BiV_{0.9925}Mo_{0.0075}O_4$, which would enhance the separation efficiency of electrons and holes. However, when t-BuOH was added, the catalytic efficiency decreased from 97.5 to 78.1%, indicating the presence of $\cdot OH$ as the active species. The photocatalytic activity was drastically reduced with the addition of $(NH_4)_2C_2O_4$, suggesting that the holes acted as the main active species.

To further confirm the main active species generated in the photocatalytic process, electron spin resonance (ESR) was used. The principle of ESR is to react with free radicals using a spin-trapping agent to generate a relatively stable free radical adduct. A peak intensity was observed under visible light compared with dark conditions (Fig. 12a), demonstrating the existence of $\cdot O^{2-}$. In
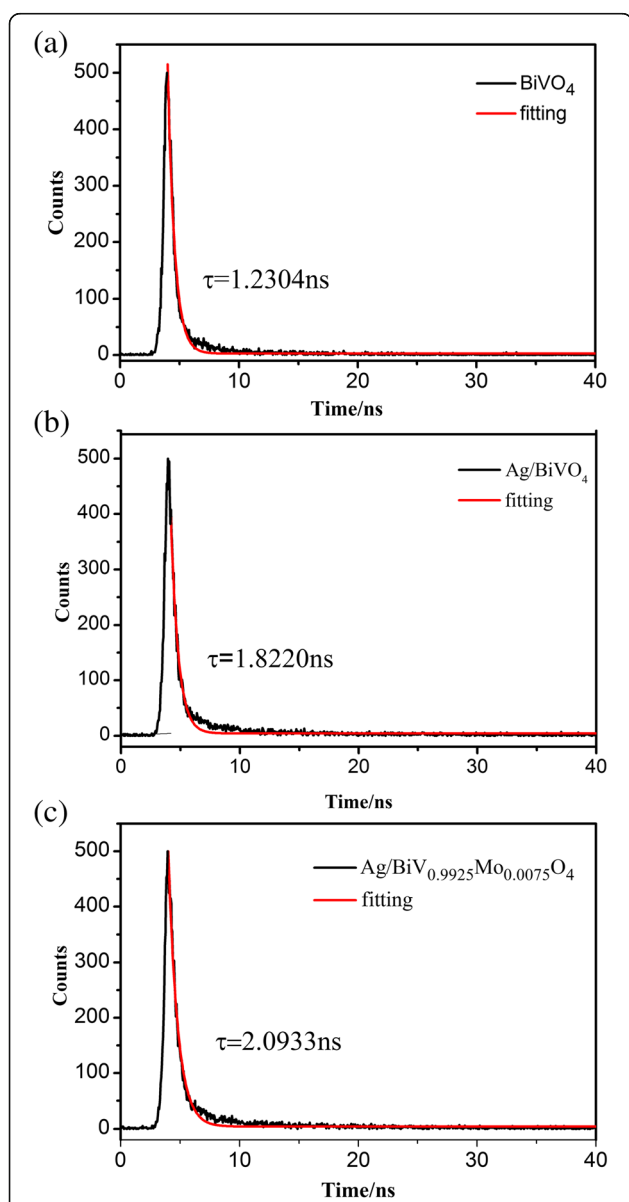

Fig. 10 Ns-level time-resolved fluorescence decay curves of as-prepared **a** $BiVO_4$, **b** $Ag/BiVO_4$, and **c** $Ag/BiV_{0.9925}Mo_{0.0075}O_4$ composite
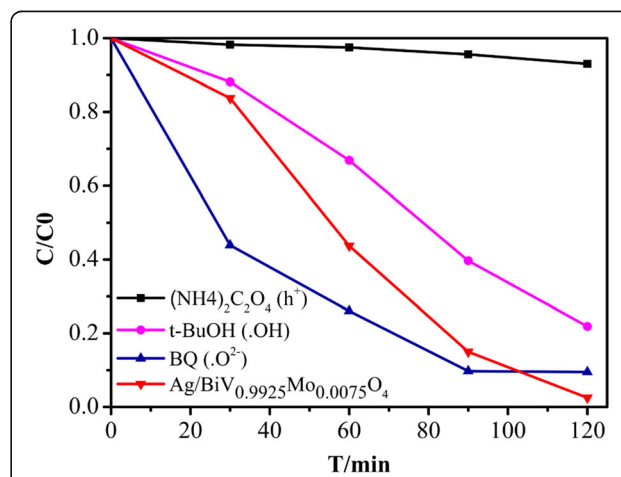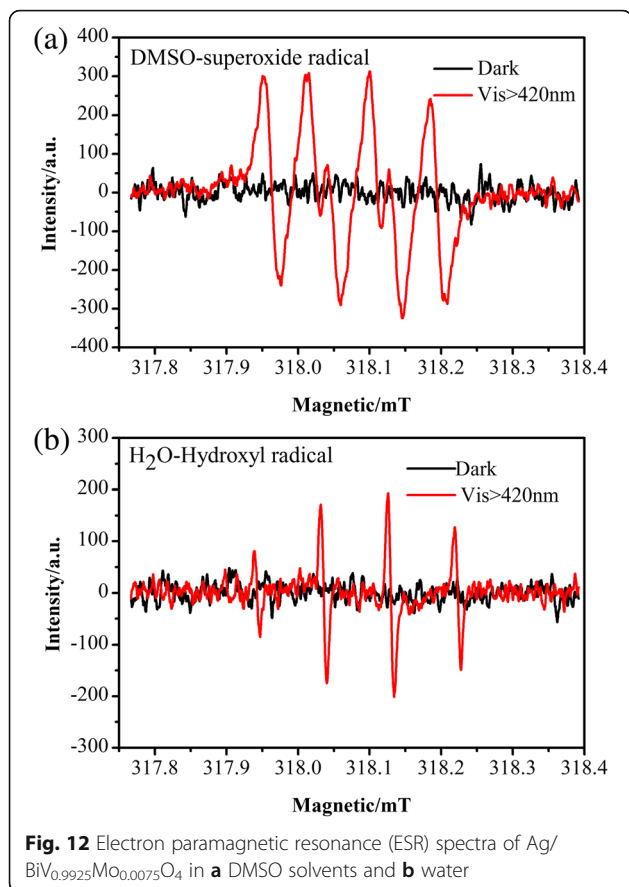

Fig. 11 Plots of photogenerated carrier trapping in the system during the photodegradation of RhB by $Ag/BiV_{0.9925}Mo_{0.0075}O_4$

Yu *et al. Nanoscale Research Letters* (2017) 12:588

Page 8 of 10

Fig. 12 Electron paramagnetic resonance (ESR) spectra of Ag/$BiV_{0.9925}Mo_{0.0075}O_4$ in **a** DMSO solvents and **b** water
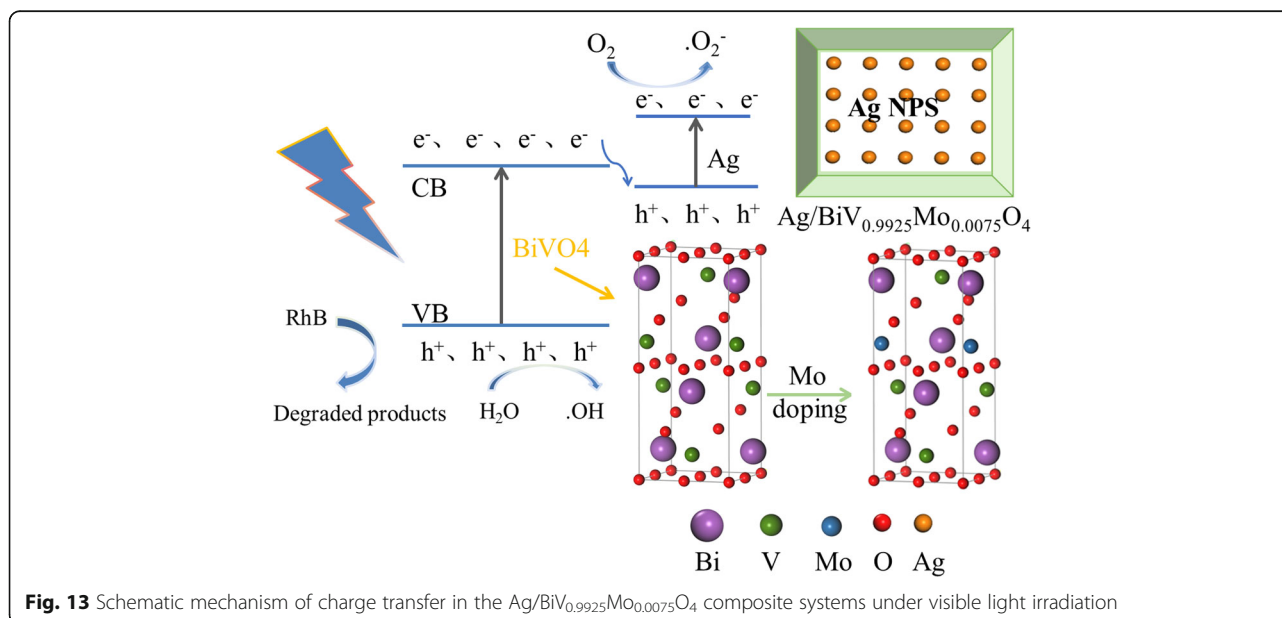
addition, obvious signals (Fig. 12b) suggested that •OH was produced in the photocatalytic process. In conclusion, the radical trap experiments and ESR analysis revealed that the photocatalytic process was governed by the combined effect of h^+, •O^{2-}, and •OH active species.

According to the discussion above, a possible photocatalytic mechanism of Ag/$BiV_{0.9925}Mo_{0.0075}O_4$ was illustrated in Fig. 13. The dopant Mo could effectively enhance the visible light absorption of the $BiVO_4$ photocatalyst. Ag/$BiV_{0.9925}Mo_{0.0075}O_4$ composite photocatalysts were irradiated under visible light, and the photoelectrons in the valence band of $BiVO_4$ could effectively jump to the conduction band to generate electron–hole pairs. The metallic Ag could accept the electrons, which then recombine with the photogenerated holes and enhance the transfer to the surface of the composite photocatalysts, resulting in the improvement of the separation of electrons and holes. The electrons could react to the O_2 and transform to •O^{2-}. The holes of $BiV_{0.9925}Mo_{0.0075}O_4$ could react with the adsorbed H_2O molecules and transform to •OH. Meanwhile, the h^+ could effectively react with the RhB, generating degraded products.

Conclusions

Herein, a simple hydrothermal synthesis procedure at almost neutral pH conditions and using ammonium carbonate as the structure-directing agent is reported for the preparation of Mo-doped $BiVO_4$ powders. Metallic Ag nanoparticles were then deposited on the (040) crystal facet of $BiV_{0.9925}Mo_{0.0075}O_4$. Thus, a photocatalytic system has been successfully constructed by means of the reduction reaction. These synthesis conditions have

Fig. 13 Schematic mechanism of charge transfer in the Ag/$BiV_{0.9925}Mo_{0.0075}O_4$ composite systems under visible light irradiation

Yu et al. Nanoscale Research Letters (2017) 12:588

Page 9 of 10

been shown to significantly influence the increase in the size of the (040) crystallographic facet, as confirmed by XRD and STEM analyses. The XRD indicated that the peak splitting observed at 30.5° is a result of the (040) facets. Ag nanoparticles deposited on the (040) facets can also be seen from the STEM. Furthermore, Ag/$BiV_{0.9925}Mo_{0.0075}O_4$ showed a highly efficient photocatalytic performance for RhB degradation under visible light irradiation. This work could offer new inspiration for the rational utilization of $BiVO_4$ photocatalysts with high photocatalytic activity and their applications in the fields of energy production and environmental protection.

Authors' contributions
XW and ZC conceived and designed the experiments. MY and SZ performed the experiments. XW, QM, MY, and GZ analyzed the data. XW contributed reagents/materials/analysis tools. All authors read and approved the final manuscript.

Competing interests
The authors declare that they have no competing interests.

Publisher's Note
Springer Nature remains neutral with regard to jurisdictional claims in published maps and institutional affiliations.

Author details
[1]South China Academy of Advanced Optoelectronics, South China Normal University, Guangzhou, Guangdong Province, China. [2]Shenyang Institute of Automation, Chinese Academy of Sciences, Guangzhou 511458, China. [3]International Academy of Optoelectronics at Zhaoqing, South China Normal University, Guangzhou, Guangdong Province, China.

References
1. Dincer I (2000) Renewable energy and sustainable development: a crucial review. Renew Sustainable Energy Rev 4:157–175
2. Huang C-K, Wu T, Huang C-W, Lai C-Y, Wu M-Y, Lin Y-W (2017) Enhanced photocatalytic performance of $BiVO_4$ in aqueous $AgNO_3$ solution under visible light irradiation. Appl Surf Sci 399:10–19
3. Ding X, Zhao K, Zhang L (2014) Enhanced photocatalytic removal of sodium pentachlorophenate with self-doped Bi_2WO_6 under visible light by generating more superoxide ions. Environ Sci Technol 48:5823–5831
4. Yang JJ, Chen DM, Zhu Y, Zhang YM, Zhu YF (2017) 3D-3D porous Bi_2WO_6/graphene hydrogel composite with excellent synergistic effect of adsorption-enrichment and photocatalytic degradation. Appl Catal B Environ 205:228–237
5. Zhu YY, Wang YJ, Ling Q, Zhu YF (2017) Enhancement of full-spectrum photocatalytic activity over $BiPO_4$/Bi_2WO_6 clomposites. Appl Catal B Environ 200:222–229
6. Tan GQ, She LN, Liu T, Xu C, Ren HJ, Xia A (2017) Ultrasonic chemical synthesis of hybrid mpg-C_3N_4/$BiPO_4$ heterostructured photocatalysts with improved visible light photocatalytic activity. Appl Catal B Environ 207:120–133
7. Bi Y, Ouyang S, Umezawa N, Cao J, Ye J (2011) Facet effect of single-crystalline Ag_3PO_4 sub-microcrystals on photocatalytic properties. J Am Chem Soc 133:6490–6492
8. Teng W, Tan XJ, Li XY, Tang YB (2017) Novel Ag_3PO_4/MoO_3 p-n heterojunction with enhanced photocatalytic activity and stability under visible light irradiation. Appl Surf Sci 409:250–260
9. Xue-lian Y, Yuan C, Bi-tao L, Ming-jing T (2016) Progress in $BiVO_4$ photocatalyst under visible light. Mater Sci Forum 852:1429–1435
10. Obregon S, Colon G (2013) On the different photocatalytic performance of $BiVO_4$ catalysts for methylene blue and rhodamine B degradation. J Mol Catal A Chem 376:40–47
11. Ng YH, Iwase A, Kudo A, Amal R (2010) Reducing graphene oxide on a visible-light $BiVO_4$ photocatalyst for an enhanced photoelectrochemical water splitting. J Phys Chem Lett 1:2607–2612
12. Kim JH, Lee JS (2014) $BiVO_4$-based heterostructured photocatalysts for solar water splitting: a review. Energy Environ Focus 3:339–353
13. Liang Y, Messinger J (2014) Improving $BiVO_4$ photoanodes for solar water splitting through surface passivation. Phys Chem Chem Phys 16:12014–12020
14. Fujishima A, Honda K (1972) Electrochemical photolysis of water at a semiconductor electrode. Nature 238:37–38
15. Zhang N, Li X, Ye H, Chen S, Ju H, Liu D, Lin Y, Ye W, Wang C, Xu Q, Zhu J, Song L, Jiang J, Xiong Y (2016) Oxide defect engineering enables to couple solar energy into oxygen activation. J Am Chem Soc 138:8928–8935
16. Reece SY, Hamel JA, Sung K, Jarvi TD, Esswein AJ, Pijpers JJ, Nocera DG (2011) Wireless solar water splitting using silicon-based semiconductors and earth-abundant catalysts. Science 334:645–648
17. Zhao J, Yan J, Jia H, Zhong S, Zhang X, Xu L (2016) $BiVO_4$/g-C_3N_4 composite visible-light photocatalyst for effective elimination of aqueous organic pollutants. J Mol Catal A Chem 424:162–170
18. Ma G, Chen Z, Chen Z, Jin M, Meng Q, Yuan M, Wang X, Liu J-M, Zhou G (2017) Constructing novel WO_3/Fe (III) nanofibers photocatalysts with enhanced visible-light-driven photocatalytic activity via interfacial charge transfer effect. Mater Today Energy 3:45–52
19. Chen F, Yang Q, Wang Y, Zhao J, Wang D, Li X, Guo Z, Wang H, Deng Y, Niu C, Zeng G (2017) Novel ternary heterojunction photcocatalyst of Ag nanoparticles and g-C_3N_4 nanosheets co-modified $BiVO_4$ for wider spectrum visible-light photocatalytic degradation of refractory pollutant. Appl Catal B Environ 205:133–147
20. Xue S, He H, Wu Z, Yu C, Fan Q, Peng G, Yang K (2017) An interesting Eu,F-codoped $BiVO_4$ microsphere with enhanced photocatalytic performance. J Alloys Compd 694:989–997
21. Zhang J, Ren F, Deng M, Wang Y (2015) Enhanced visible-light photocatalytic activity of a g-C_3N_4/$BiVO_4$ nanocomposite: a first-principles study. Phys Chem Chem Phys 17:10218–10226
22. Zhou Y, Li W, Wan W, Zhang R, Lin Y (2015) W/Mo co-doped $BiVO_4$ for photocatalytic treatment of polymer-containing wastewater in oilfield. Superlattice Microst 82:67–74
23. Wang K, Liang L, Liu H, Xie X, Hao Q, Liu C (2015) Facile synthesis of hollow and porous Ag^+/Ag/$BiVO_4$ composite fibers with enhanced visible-light photocatalytic performance. Mater Lett 161:336–339
24. Wang J, Shi W, Liu D, Zhang Z, Zhu Y, Wang D (2017) Supramolecular organic nanofibers with highly efficient and stable visible light photooxidation performance. Appl Catal B Environ 202:289–297
25. Pattengale B, Huang J (2016) The effect of Mo doping on the charge separation dynamics and photocurrent performance of $BiVO_4$ photoanodes. Phys Chem Chem Phys 18:32820–32825
26. Antony RP, Baikie T, Chiam SY, Ren Y, Prabhakar RR, Batabyal SK, Loo SCJ, Barber J, Wong LH (2016) Catalytic effect of Bi^{5+} in enhanced solar water splitting of tetragonal $BiV_{0.8}Mo_{0.2}O_4$. Appl Catal A 526:21–27
27. Seabold JA, Zhu K, Neale NR (2014) Efficient solar photoelectrolysis by nanoporous Mo: $BiVO_4$ through controlled electron transport. Phys Chem Chem Phys 16:1121–1131
28. Parmar KPS, Kang HJ, Bist A, Dua P, Jang JS, Lee JS (2012) Photocatalytic and photoelectrochemical water oxidation over metal-doped monoclinic $BiVO_4$ photoanodes. ChemSusChem 5:1926–1934
29. Thalluri SM, Hernandez S, Bensaid S, Saracco G, Russo N (2016) Green-synthesized W- and Mo-doped $BiVO_4$ oriented along the {040} facet with enhanced activity for the sun-driven water oxidation. Appl Catal B Environ 180:630–636
30. Luo W, Wang J, Zhao X, Zhao Z, Li Z, Zou Z (2013) Formation energy and photoelectrochemical properties of $BiVO_4$ after doping at Bi^{3+} or V^{5+} sites with higher valence metal ions. Phys Chem Chem Phys 15:1006–1013
31. Qiao R, Mao M, Hu E, Zhong Y, Ning J, Hu Y (2015) Facile formation of mesoporous $BiVO_4$/Ag/AgCl heterostructured microspheres with enhanced visible-light photoactivity. Inorg Chem 54:9033–9039

Yu *et al. Nanoscale Research Letters* (2017) 12:588

Page 10 of 10

32. Gao XM, Wu YF, Wang J, Fu F, Zhang LP, Niu FX (2012) The preparation of Cu-BiVO$_4$ and its enhanced photocatalytic properties for degradation of Phenol. Adv Mater Res 356:1253–1257
33. Hirakawa H, Shiota S, Shiraishi Y, Sakamoto H, Ichikawa S, Hirai T (2016) Au nanoparticles supported on BiVO$_4$: Effective inorganic photocatalysts for H$_2$O$_2$ production from water and O$_2$ under visible light. ACS Catal 6:4976-4982
34. Li J, Zhou J, Hao H, Zhu Z (2016) Silver-modified specific (040) facet of BiVO$_4$ with enhanced photoelectrochemical performance. Mater Lett 170:163–166
35. Yao W, Iwai H, Ye J (2008) Effects of molybdenum substitution on the photocatalytic behavior of BiVO$_4$. Dalton Trans 11:1426–1430
36. Pilli SK, Furtak TE, Brown LD, Deutsch TG, Turner JA, Herring AM (2011) cobalt-phosphate (Co-Pi) catalyst modified Mo-doped BiVO$_4$ photoelectrodes for solar water oxidation. Energy Environ Sci 4:5028–5034
37. Li R, Zhang F, Wang D, Yang J, Li M, Zhu J, Zhou X, Han H, Li C (2013) Spatial separation of photogenerated electrons and holes among {010} and {110} crystal facets of BiVO$_4$. Nat Commun 4:1432–1438
38. Ni Z, Dong F, Huang H, Zhang Y (2016) New insights into how Pd nanoparticles influence the photocatalytic oxidation and reduction ability of g-C$_3$N$_4$ nanosheets. Catal Sci Technol 6:6448–6458
39. Chen F, Yang Q, Li X, Zeng G, Wang D, Niu C, Zhao J, An H, Xie T, Deng Y (2017) Hierarchical assembly of graphene-bridged Ag$_3$PO$_4$/Ag/BiVO$_4$ (040) Z-scheme photocatalyst: An efficient, sustainable and heterogeneous catalyst with enhanced visible-light photoactivity towards tetracycline degradation under visible light irradiation. Appl Catal B Environ 200:330–342
40. Chen F, Yang Q, Niu C, Li X, Zhang C, Zhao J, Xu Q, Zhong Y, Deng Y, Zeng G (2016) Enhanced visible light photocatalytic activity and mechanism of ZnSn(OH)$_6$ nanocubes modified with AgI nanoparticles. Catal Commun 73:1–6
41. Dong G, Ho W, Zhang L (2015) Photocatalytic NO removal on BiOI surface: the change from nonselective oxidation to selective oxidation. Appl Catal B Environ 168:490–496